Desalination and Water Treatment
www.deswater.com

doi: 10.1080/19443994.2014.901191

54 (2015) 502–510
April

Taylor & Francis
Taylor & Francis Group

Synthesis and characterization of coated zero-valent iron nanoparticles and their application for the removal of aqueous Pb^{2+} ions

Yue Cheng[a,b,*], Chuang Jiao[a,b], Wenjing Fan[a,b]

[a] *School of Materials Science and Engineering, Jingdezhen Ceramic Institute, Jingdezhen 333403, Jiangxi Province, China, Tel. +86 798 8499678; Fax: +86 798 8491446; email: cy_jci@163.com*
[b] *Key Laboratory of Jiangxi Province for Advanced Ceramic Materials, Jingdezhen 333001, Jiangxi Province, China*

Received 16 October 2013; Accepted 1 March 2014

ABSTRACT

Three types of coated nanoscale zero-valent iron (C-nZVI) with different coatings, agar, starch, and carboxyl methyl cellulose, were synthesized using a rheological phase reaction method. The structure and morphology of C-nZVI particles were characterized by X-ray powder diffraction, scanning electron microscopy, and transmission electron microscopy. Batch tests of Pb(II) removal showed that the sample dosage, initial pH, initial Pb(II) concentration, and reaction time have significant effects on Pb(II) removal efficiency. Experimental results proved that an optimized pH value of 5, Pb(II) concentration of 100 mg/L, and C-nZVI dosage of 1 g/L are beneficial to Pb(II) removal. Kinetic study revealed that Pb (II) removal by C-nZVI in aqueous solution complies with quasi-first-order reaction kinetics, and the reaction rate constant of Pb(II) removal using W-nZVI is 6–27 higher than using unwrapped nZVI.

Keywords: Rheological phase reaction; Carboxyl methyl cellulose; Agar- and starch-coated nanoscale zero-valent iron; Pb(II) removal

1. Introduction

Lead (Pb) is widely distributed in nature, and commonly used in industrial processes [1–3]. Pb and its compounds are stable and non-biodegradable pollutants and are released into environment through wastewater, waste gas, and other paths. Industrial wastewater containing Pb is permeable to soil, polluting rivers, destroying soil ecosystem, affecting crop growth, and proliferation of biological populations. Pb mainly accumulates in human muscles, bones, kidneys, and brain tissue which relates to anemia, nervous system disorders, and kidney disease [4–6]. Pb removal plays a critical role in wastewater treatment.

Conventional chemical precipitation, ion exchange, filtration, adsorption, and reverse osmosis are being used to remove heavy metals from water [7]. Among these methods, adsorption and chemical precipitation are highly efficient and economical [8]. However, there are some drawbacks among a variety of methods for Pb removal [9].

Nanoscale zero-valent iron (nZVI) has shown good potential to remove heavy metals and other aqueous pollutants. Its physicochemical properties and reductive capacity facilitate rapid decontamination of wastewater [10,11]. Unfortunately, nZVI aggregates easily and its efficiency is easily decreased by reduced surface

---

*Corresponding author.

area, producing a less negative oxidation–reduction potential [12]. Several strategies have been applied to stabilize the synthesized iron nanoparticles. Anionic hydrophilic carbon [13] and chitosan/silica [14] were successfully employed as supporters to inhibit the aggregation of iron nanoparticles. Huang et al. [15] proved that iron nanoparticles were immobilized onto supported polyelectrolyte multilayers and yielded nanoparticles with evenly distributed sizes (1–4 nm).

Many methods have been used for the preparation of nZVI including chemical vapor deposition, inert gas condensation, pulsed laser ablation, spark discharge generation, sputtering gas-aggregation, thermal decomposition, thermal reduction of oxide compounds, hydrogenation of metallic complexes, and aqueous reduction of iron salts [16]. The properties of metallic nanoparticles are influenced by its composition and microstructure, which are sensitive to the preparation methodology.

nZVI synthesis involves liquid phase reduction because the synthesis process only requires simple, mild reaction conditions, which is achievable in laboratory. However, synthesis of nZVI using these methods involves an inert reduction atmosphere and a series of complicated technologies and increases the costs of production.

The rheological phase reaction method is a process for preparing compounds or materials from a solid–liquid rheological mixture. There are many advantages in the rheological phase system, such as efficient utilization of solid particle surface area, close and uniform contact between solid particle and fluid, good heat exchange, and good reaction temperature control. With this approach, many functional materials and compounds with novel structures have been synthesized [17].

Coated nanoscale zero-valent iron (C-nZVI) were prepared with cheap and harmless sodium carboxymethyl cellulose (CMC), agar (Agar), and water-soluble starch (Starch) as surface modifier by rheological phase reaction method; samples were characterized and analyzed by X-ray powder diffraction (XRD), scanning electron microscopy (SEM), and transmission electron microscopy (TEM). The effects of sample dosage, Pb(II) initial concentration, reaction time, and pH value on Pb removal are investigated in this paper.

2. Materials and methods

2.1. Preparation of nZVI

The stabilized nZVI was synthesized by mixing $FeSO_4 \cdot 7H_2O$ (CAS No: 7782-63-0) and KBH_4 (CAS No: 13762-51-1) with a molar ratio of 1:3 and was then grinded in agate mortar. The solid mixture was added to an agar solution to form a rheological body, and the mixture was then transferred into a three-necked round-bottom flask. The reaction was conducted with continuous stirring at room temperature. The solid phase product was collected by filtration, washed with deionized water and ethanol, and finally dried at 100˚C under vacuum condition.

2.2. Preparation of C-nZVI

C-nZVI was prepared using rheological phase reaction method as follows:

(1) $FeSO_4 \cdot 7H_2O$ and KBH_4 were mixed with the molar ratio of 1:3 by grinding in an agate mortar for 10 min; then the solid phase medium was obtained;

(2) 0.06 g/mL sodium carboxymethyl cellulose (CMC); (CAS No. 9004-32-4), agar (Agar); (CAS No. 9002-18-0), and soluble starch (Starch); (CAS No. 9005-84-9) in aqueous solution were prepared as the liquid medium;

(3) The liquid medium was added to solid phase medium with the solid–liquid weigh ratio of 1:2, and then was stirred uniformly into rheological phase for 2 h at room temperature; the reaction system was as follows:

$$Fe^{2+} + 2BH_4^- + 6H_2O \rightarrow Fe + 2B(OH)_3 + 7H_2 \qquad (1)$$

(4) The reaction product was washed three times with 50 mL of ethanol, and then was dried at 100˚C in a vacuum oven.

2.3. Characterization and analysis

The XRD patterns were scanned using a Bruker D8 Advance Diffractometer (Bruker, Germany) with Cu Ka radiation from 5˚ to 70˚ at a rate of 0.2˚/s. The tube current was 100 mA and the tube voltage is 40 kV. The structure and morphology of C-nZVI particles were investigated by SEM on a high-resolution scanning electron microscopy (JEOL-JMS-6700F, Japan) with an acceleration voltage of 10–30 kV. The micro morphology was characterized by TEM on a high-resolution transmission electron microscope (HR-TEM, JEOL JEM-2010, Japan) with an acceleration voltage of 200 kV.

2.4. Pb(II) removal trial design

2.4.1. Pb(II) removal test

Pb nitrate solution was used as simulated wastewater and Pb(II) removal test was proceeded in 500 mL of grinding mouth stopper conical flasks. 200 mL Pb(II) with different initial concentrations was added to the conical flask, pH was adjusted, and then C-nZVI samples with different qualities were added and were stirred with magnetic stirring apparatus at 200 rpm in the flask under room temperature and atmospheric pressure. After a certain time, the solutions were filtered using a 0.22 μm filter membrane to separate the solid particles and solution. The concentrations of Pb(II) were determined by flame atomic absorption spectrometry, using a 361MC (Shanghai instrument analysis instrument Co., Ltd) atomic absorption spectrometer equipped with an air-acetylene burner and controlled by Intel Pentium four personal computer. The hollow cathode lamp was operated at analytical wavelength of 283.3 nm for Pb(II) and slit width as 0.2 nm for metal ions [18].

2.4.2. Kinetics study

The reaction of nZVI with Pb(II) in solution is a heterogeneous reaction, which can be described with Langmuir–Hinshelwood kinetic model as follows [19].

$$v = -\frac{dC}{dt} = \frac{KbC}{1 + bC} \tag{2}$$

where K: solid surface reaction rate constant; b: constant of associated with solid adsorption heat and temperature.

When the reactant concentration is low, $bC \leq 1$, (2) can be written as:

$$v = -\frac{dC}{dt} = KbC = kC \tag{3}$$

where $k = Kb$, the reaction reduced to a first-order reaction. After an evaluation of integrals Eq. (3) can be written as:

$$\ln\left(\frac{C}{C_0}\right) = k_{\text{obs}} t \tag{4}$$

$\ln(C/C_0)$ and time t is linear relationship, the slope k_{obs} is the apparent rate constant.

3. Results and discussion

3.1. Characterization of the composite

3.1.1. XRD analysis

The XRD patterns of nZVI, agar-nZVI, starch-nZVI, and CMC-nZVI are shown in Fig. 1(a)–(d), respectively. It can be seen that four samples, all present nZVI diffraction peaks at $2\theta = 44.8^\circ$ and 65.3°, which coincides with the standard body-centered cubic lattice iron diffraction peak. Notice that in Fig. 1(d), besides nZVI peaks, another K^+ diffraction peak also appeared at $2\theta = 30.1^\circ$ and 31.2°. As K^+ can be bonded with CMC, and also because K^+ is not soluble in alcohol, K^+ can be detected in the sample. In addition, no strong signals for iron oxides ($2\theta = 35.46^\circ$, 43.12°, 53.50°, 56.98°, and 62.64°) were observed, indicating Fe oxide in the sample is very small and the sample has high purity.

3.1.2. SEM analysis

The SEM images of nZVI, agar-nZVI, starch-nZVI, and CMC-nZVI are shown in Fig. 2(a)–(d), respectively. As shown in Fig. 2(a), it can be observed that nZVI particle, diameters of 50–100 nm exist in contact with each other and aggregate stack. Although they are called "zero-valent iron nanoparticles", it should be noted that the spherical iron particles form aggregate stack which might be larger than a micron rather than existing in separate nanoparticles [20]. The SEM image of agar-nZVI, starch-nZVI, and CMC-nZVI are presented in Fig. 2(b)–(d), respectively. Chain-like aggregations of iron nanoparticles still exist, but, unlike pure nZVI, these images show that separation

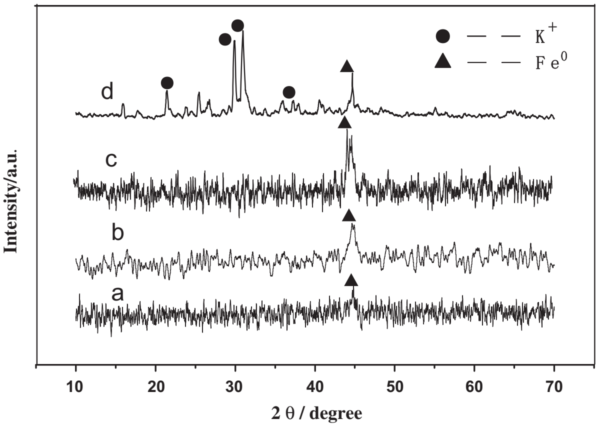

Fig. 1. The XRD spectra of different kinds of nZVI by a rheological phase reaction method (a) nZVI, (b) agar-nZVI, (c) starch-nZVI, and (d) CMC-nZVI.

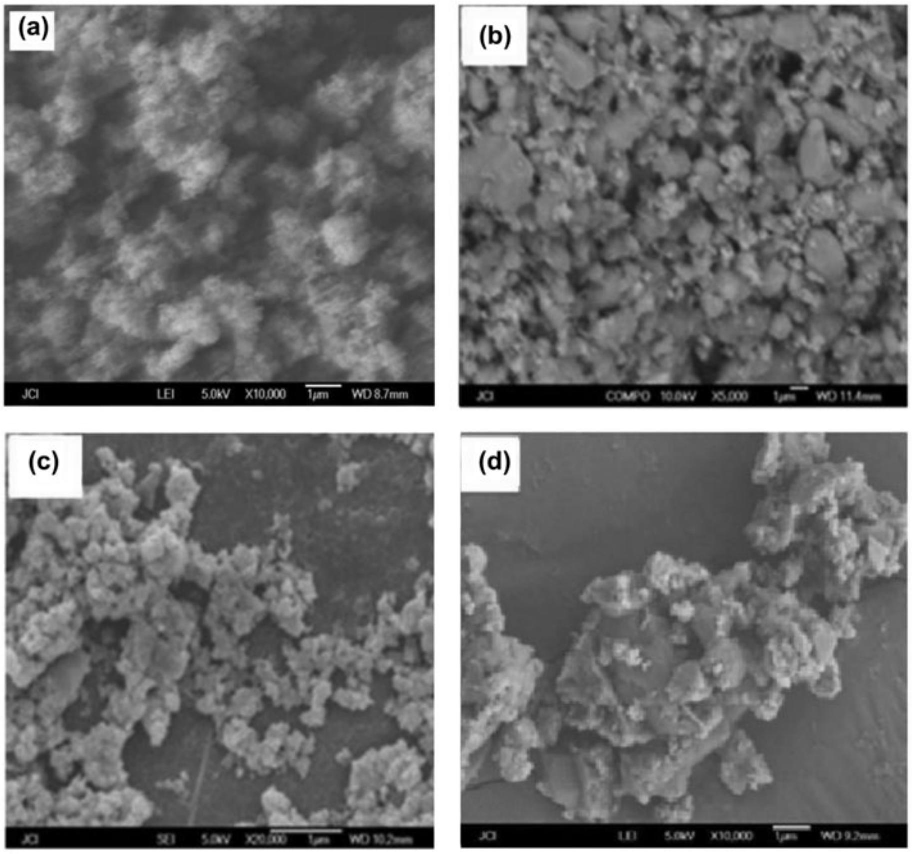

Fig. 2. The SEM spectrogram of (a) nZVI, (b) agar-nZVI , (c) starch-nZVI, and (d) CMC-nZVI.

of spherical iron nanoparticles is possible in the presence of an organic dispersing agent (agar, starch, and CMC). Similar to this, results were reported using CMC as the stabilized material [21]. The white spots in Fig. 2(b)–(d) represent agar-nZVI, starch-nZVI, and CMC-nZVI particles. It is shown that the particles were distributed evenly, had good dispersion and didn't have particle agglomeration due to the good dispersion properties of particles or agar, starch, or CMC surface preventing particles from agglomeration.

3.1.3. TEM analysis

Fig. 3(a) is nZVI (60°C vacuum dried) TEM photographs. It can be seen from the figure, that the individual particles remain spherical or ellipsoidal, with the particle diameter of about 30–50 nm, presented in a chain or agglomeration piles. Because of the attraction from the ground force, the static force between the small particles and the surface tension and the surface effects of ultrafine particles tend to aggregate. Fig. 3(b)–(d) are TEM photographs of agar-nZVI, starch-nZVI, and CMC-nZVI, respectively. From Fig. 3(b)–(d), it can be clearly seen that the nanoparticles are either spherical or elliptical, and wrapped by gray agar-, starch-, and CMC-layers, effectively preventing agglomeration of nano-iron particles. This is mainly because iron nanoparticles surface is covered by electrically charged layers (agar-, starch-, and CMC-layers) forming electrostatic repulsion and steric effect between molecules, making nanoscale iron particles separate from each other hence the, dispersion of nanoscale iron was improved [22]. The average diameters of separated iron nanospheres of agar-nZVI, starch-nZVI, and CMC-nZVI can also be observed as 50–100 nm, 8–20 nm, and 80–100 nm, respectively.

In addition, potassium borate and ferrous sulfate were ground into fine powder prior to rheological phase reaction. The parcel agent solution was then added and formulated into rheological phase. Because rheological phase has complex chemical composition or structure, and solid particles and liquid could both exist, and it could display combined solid–liquid phase properties at the same time, which overcomes hard aggregates generated during wet preparation process and further improved the dispersion of nanoscale iron particles.

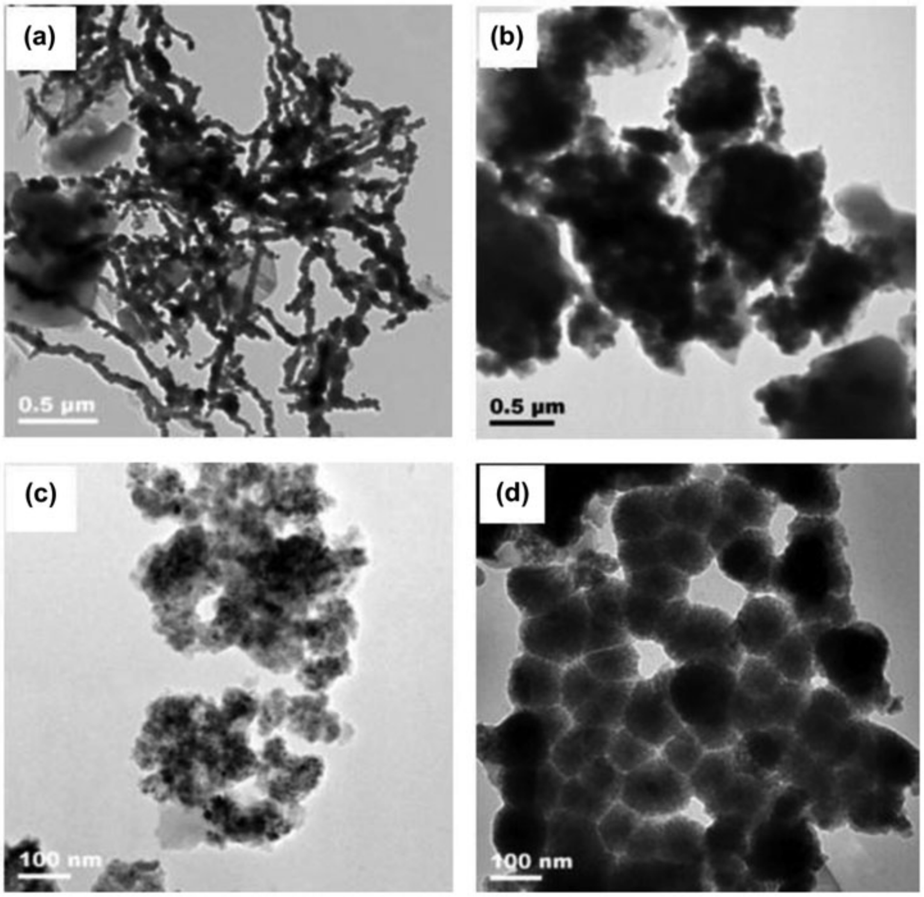

Fig. 3. The TEM spectrogram of (a) nZVI, (b) agar-nZVI, (c) starch-nZVI, and (d) CMC-nZVI.

3.2. Removal of Pb(II) from water

3.2.1. Coatings effects on Pb(II) removal

As a reductant and adsorbent, nZVI properties play an important role in Pb(II) removal reaction. To compare the effects of different coatings to Pb(II) removal, nZVI, agar-nZVI, CMC-nZVI, and starch-nZVI, each with a dosage of 0.75 g/L were applied. Concentration of Pb(II) is 200 mg/L and pH was adjusted to 5.0 for all cases [23]. Then the solutions were stirred with 200 rpm at room temperature. Solutions were sampled at certain time points (5, 10, 20, 30, 60, 90, 120, 180, and 240 min), the remaining Pb(II) concentrations were examined and compared between different warping agents.

Fig. 4 shows that 100% Pb(II) was removed using three types of coated nZVI (agar-nZVI, starch-nZVI, and CMC-nZVI. During the first 30 min, removal efficiencies reached 94.8, 96.5, and 98.81% for agar-nZVI, starch-nZVI, and CMC-nZVI, respectively, coated but Pb(II) removal rate for nZVI is relatively low, which is

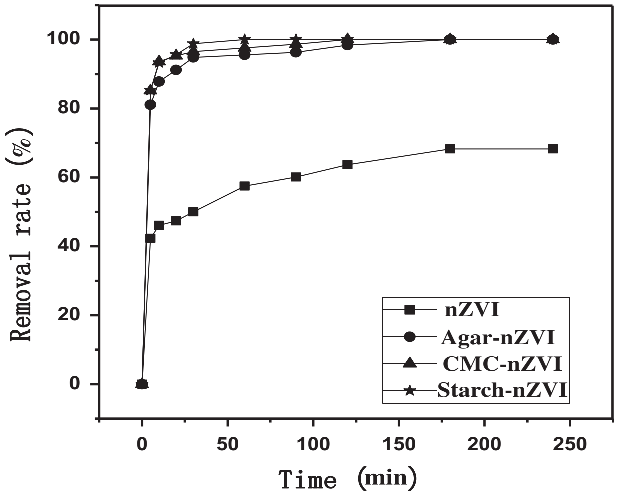

Fig. 4. Disappearance of Pb(II) in the presence of unsupported and supported iron nanoparticles.

only 68.3%. Coated agent to nZVI particles increased dispersibility to nZVI particles, and nZVI particles can well suspend in liquid phase, which avoided particle agglomeration and enhanced contact between agents and Pb(II). C-nZVI-uncoated nZVI could easily form a chain or gather in piles, which is not beneficial for contact and the reaction activity with the contaminants.

3.2.2. Effect of initial pH

pH is an important factor for Pb(II) removal in this study. It is widely accepted that low pH has a negative effect on metal adsorption by nZVI. When pH is lower than the isoelectric point of nZVI, the positive charge surface will repulse metal cations [24]. Moreover, Fe^0 will dissolve very rapidly at low pH [25]. In order to study the effects of initial PH on Pb(II) removal using C-nZVI (agar-nZVI, CMC-nZVI, and starch-nZVI, the solution pH was adjusted to 3.0, 4.0, 5.0, and 6.0 with initial Pb(II) concentration of 200 mg/L and C-nZVI dosage of 0.5 g/L, respectively. It is shown in Fig. 5 that Pb(II) removal efficiencies using agar-nZVI, CMC-nZVI, and starch-nZVI were affected by initial pH. Specifically, Pb(II) removal efficiencies increased when pH increased, but reached the maximum (100%) when pH reached 5.0 and further decreased when pH was higher than 5.0. The reaction tended to move to reductive direction when pH increased before reaching 5.0, which enhanced the Pb(II) reduction. But when pH decreased, H^+ in solution will be abundant and tend to react with Fe^0, which inhibited the reduction reaction. When pH is higher than pH, iron hydroxide or carbonate iron oxide film will be easily formed on the surface of nZVI, which decreased the nZVI activity and had negative effect on Pb(II) reduction reaction [26,27]. Generally speaking, the effects of solution initial pH on Pb (II) removal was a combination of various mechanisms for the reduction process.

3.2.3. Pb(II) removal of different Pb(II) initial concentration

Different Pb(II) concentrations could also affect the contact between the reactants and further affect Pb(II) removal efficiency. To examine the effects of initial Pb(II) concentration on Pb(II) removal by agar-nZVI, CMC-nZVI, and starch-nZVI, the initial pH of the solution, the dosage of the coated nZVI were set as 5.0 and 0.5 g/L respectively, and the initial Pb(II) concentrations were set as 100, 150, 200, 250, and 300 mg/L, respectively.

Fig. 6 shows that, when initial Pb(II) concentration increased, Pb(II) removal efficiencies decreased with all three types of C-nZVI. The three C-nZVI samples completely removed Pb(II) when initial Pb(II) was 100 mg/L; then the removal efficiency dropped to less than 80% when the initial Pb(II) concentration increased to 300 mg/L. Higher Pb(II) concentration reduced the active sites on C-nZVI for reduction reaction, which could be the cause of removal efficiency decreasing. Similar result was reported by Zhang et al. [28] about Pb removal with kaolin supported nZVI.

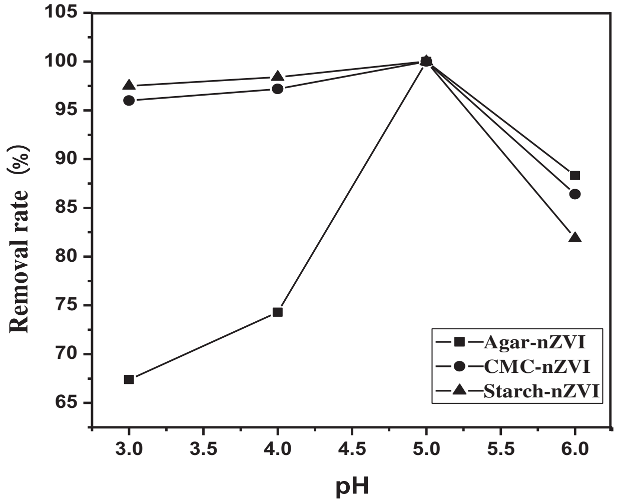

Fig. 5. Removal rate of Pb(II) in the aqueous phase at various pH values.

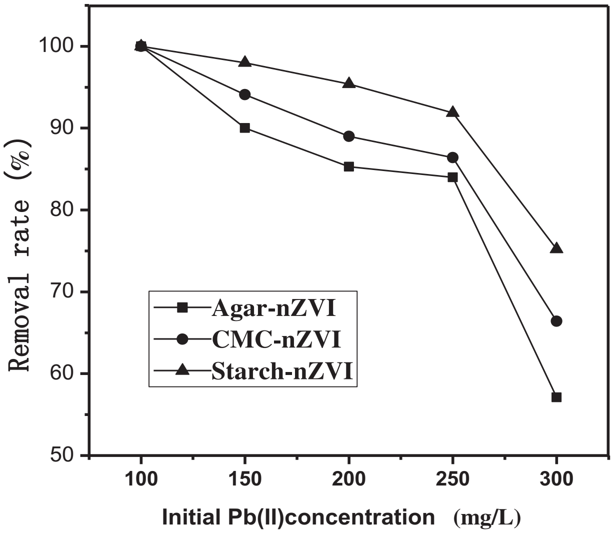

Fig. 6. Removal rate of Pb(II) at various initial Pb(II)concentration.

In order to study of the sample dosage of C-nZVI for Pb(II) removal, four levels of sample dosages (0.25, 0.5, 0.75, and 1 g/L), were tested with initial pH value set as 5.0, the Pb(II) initial concentration set as 200 mg/L and the reaction set as 120 min.

It is shown in Fig. 7, Pb(II) removal efficiency was increased when sample dosages increased within the tested range, and reaches 100% when the dosage was 1 g/L. This is because higher sample concentration increased its active site on the sample surface, and increased the contacts between fresh Fe surface and the Pb(II). It is concluded that the dosage of W-nZVI is a major controlling factor at low dosage, when Pb (II) removal efficiency reached a certain point, sample dosage will no longer be a control factor. This result corresponds to the result in Yun et al. [29].

3.3. Pb(II) removal reaction kinetics study

Pb(II) removal kinetics with nZVI, agar-nZVI, CMC-nZVI, and starch-nZVI were studied when ph was 5.0, initial Pb(II) concentration was 200 mg/L and sample dosages were all 0.75 g/L. It can be seen from Fig. 8, for all types of nZVI samples, a good linear relationship was shown between $\ln(C/C_0)$ and time t, in which C and C_0 are the final and initial Pb(II) concentrations, respectively. It was showed that all warping materials examined in this study didn't affect the kinetics of Pb(II) removal processes, but they did increase the reaction rate constant (Table 1). W-nZVI considering the reaction rate constants (k_{obs}) for specific-coated nZVI, k_{obs} of starch-nZVI, agar-nZVI, CMC-nZVI, and nZVI is 0.0934, 00244, 0.0187, and 0.0034 min^{-1}, respectively. The reaction rate constant of W-nZVI-k_{obs} is 6–27 times of the unwrapped nZVI, this result is consistent with result from Ponder et al. [30]

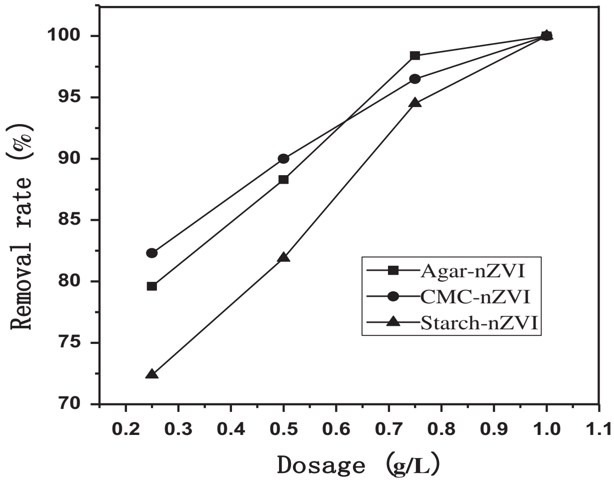

Fig. 7. Removal rate of Pb(II) at various dosages.

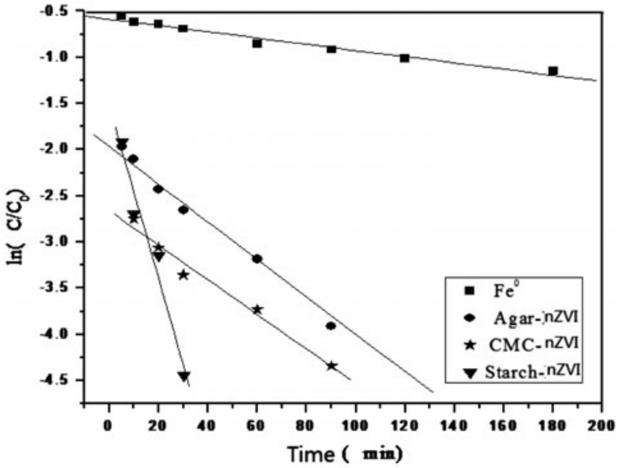

Fig. 8. Dynamics curve for treatment of Pb(II) by nZVI.

Table 1
The apparent reaction rate constant of the removal of Pb(II) by nZVI

Samples	k_{obs}/ (min)	R^2	Wk_{obs}
nZVI	0.0034	0.9659	/
CMC-nZVI	0.0187	0.9803	5.50
Agar-nZVI	0.0244	0.9245	7.18
Starch-nZVI	0.0934	0.9587	27.47

Note: Wk_{obs} = W-nZVI-k_{obs}/nZVI-k_{obs}.

3.4. Reaction mechanism of coated Pb(II) removal by C-nZVI

Nanoparticles were uniformly dispersed in the solution when Pb(II) removal reaction took place with coated nZVI. The surface of the coatings began to dissolve after a certain time, and as a result, nZVI began to expose slowly and reacted with oxygen in the solution as follows [31]:

$$\text{Coated} - \text{Fe}^0 \rightarrow \text{coated} + \text{nZVI}\,(\text{release}) \quad (5)$$

$$2\text{Fe}^0 + 4\text{H}^+ + \text{O}_2 \rightarrow 2\text{Fe}^{2+} + 2\text{H}_2\text{O}\,(\text{acidic solution}) \quad (6)$$

$$\text{Fe}^0 + 2\text{H}_2\text{O} \rightarrow \text{Fe}^{2+} + \text{H}_2 + 2\text{OH}^- \quad (7)$$

Since nZVI has large surface area and can strongly absorb Pb(II), the other part of nZVI may absorb a large number of Pb(II) on the surface of nZVI. This process will generate Pb^0 and the reaction process is described as follows [28]:

$$Pb^2 + \text{package agent-}Fe^0 \rightarrow Pb^{2+}\text{- coated agent-FeO (adsorption)} \quad (8)$$

$$3Pb^{2+} + 2nZVI + 4H_2O \rightarrow 3Pb^0 + 2FeOOH + 2H^+ \quad (9)$$

In addition, part of the Pb(II) will contact with OH^- on NZVI surface to form ligand ($Pb(OH)_2$ and $PbO{\cdot}xH_2O$), which can be described as follows [30]:

$$Pb^{2+} + OH^- \rightarrow Pb(OH)_2 + PbO \cdot xH_2O \quad (10)$$

4. Conclusions

A ratio of $FeSO_4{\cdot}7H_2O$: $KBH_4 = 1{:}3$ (molar ratio) as a solid phase medium, a concentration of 0.06 g/mL coating material solution as the liquid medium, a solid–liquid reaction ratio of 1:2, and 2 h reaction time at room temperature were determined as the optimized condition for preparing the C-nZVI. agar-nZVI particle size ranges from 50 to 100 nm and particle distribution in solution is evenly distributed. No agglomeration was observed during operation indicating good dispersion property. It also shows good inoxidizability; CMC-nZVI uniform particle distribution, particles is separated from each other, showing a discrete state but not connected to each other, particle size of 80–100 nm; and starch-nZVI particle size of 8–20 nm.

Experimental results show that the optimum pH value of 5, lower initial Pb(II) concentration, and a higher dosage of samples benefit Pb(II) removal. Kinetics study shows Pb(II) removal by C-nZVI complies with quasi-one reaction kinetics; C-nZVI with four different warping materials showed greater Pb(II) removal reaction rate constants than the nZVI.

Acknowledgments

This work has been funded by the National Natural Science Foundation of China (No. 51268018) and Visiting Scholar of Jiangxi University of Young Teacher Development Programs Project. The authors are grateful to the National Engineering Research Center for Domestic and Building Ceramic, JCU for the assistance in the analytical measurements.

References

[1] H.N. Bhatti, A. Saleem, M.A. Hanif, Utilization of *Mentha arvensis* waste biomass for the removal of Pb (II) and Co(II) from aqueous solutions, Desalin. Water Treat. 51 (2013) 3335–3343.

[2] C. Saka, O. Şahin, H. Demir, M. Kahyaoğlu, Removal of lead(II) from aqueous solutions using pre-boiled and formaldehyde-treated onion skins as a new adsorbent, Sep. Sci. Technol. 46 (2011) 507–517.

[3] F. Boudrahem, F. Aissani-Benissad, A. Soualah, Adsorption of lead(II) from aqueous solution by using leaves of date trees as an adsorbent, J. Chem. Eng. Data 56 (2011) 1804–1812.

[4] F. Aydin, F. Yasar, I. Aydin, F. Guzel, Determination of lead separated selectively with ion exchange method from solution onto BCW in Sirnak, East Anatolia of Turkey, Microchem. J. 98 (2011) 246–253.

[5] M. Khajeh, Z.S. Heidari, E. Sanchooli, Synthesis, characterization and removal of lead from water samples using lead-ion imprinted polymer, Chem. Eng. J. 166 (2011) 1158–1163.

[6] D.M. Roundhill, Novel strategies for the removal of toxic metals from soils and waters, J. Chem. Educ. 81 (2004) 275–282.

[7] US EPA, Cost and benefits of reducing lead in gasoline, Draft Final Report, Office of Policy Analysis, US EPA 230-03-84-005, Washington, DC, 1984.

[8] F. Fu, Q. Wang, Removal of heavy metal ions from wastewaters: A review, J. Environ. Manage. 92 (2011) 407–418.

[9] M.K. Mondal, Removal of Pb(II) ions from aqueous solution using activated tea waste: Adsorption on a fixed-bed column, J. Environ. Manage. 90 (2009) 3266–3271.

[10] R. Singh, V. Misra, R.P. Singh, Synthesis, characterization and role of zero-valent iron nanoparticle in removal of hexavalent chromium from chromium-spiked soil, J. Nanopart. Res. 13 (2011) 4063–4073.

[11] L. Alidokht, A.R. Khataee, A. Reyhanitabar, S. Oustan, Reductive removal of Cr(VI) by starch-stabilized Fe0 nanoparticles in aqueous solution, Desalination 270 (2011) 105–110.

[12] F. He, D. Zhao, Preparation and characterization of a new class of starch-stabilized bimetallic nanoparticles for degradation of chlorinated hydrocarbons in water, Environ. Sci. Technol. 39 (2005) 3314–3320.

[13] B. Schrick, B.W. Hydutsky, J.L. Blough, T.E. Mallouk, Delivery vehicles for zerovalent metal nanoparticles in soil and groundwater, Chem. Mater. 16 (2004) 2187–2193.

[14] B.W. Zhu, T.T. Lim, J. Feng, Reductive dechlorination of 1,2,4-trichlorobenzene with palladized nanoscale Fe0 particles supported on chitosan and silica, Chemosphere 65 (2006) 1137–1145.

[15] Q.G. Huang, X.Y. Shi, R.A. Pinto, E.J. Petersen, W.J. Weber, Tunable synthesis and immobilization of zero-valent iron nanoparticles for environmental applications, Environ. Sci. Technol. 42 (2008) 8884–8889.

[16] R.A. Crane, T.B. Scott, Nanoscale zero-valent iron: Future prospects for an emerging water treatment technology, J. Hazard. Mater. 211–212 (2012) 122–125.

[17] J. Jiang, L. Li, F. Xu, Y. Xie, Preparation and magnetic properties of Zn–Cu–Cr–Sm ferrite via a rheological

phase reaction method, Mater. Sci. Eng. B-Adv. 137 (2007) 166–169.

[18] N. Khalid, S. Rahman, Adsorptive removal of lead from battery wastewater by coconut coir, Sep. Sci. Technol. 45 (2010) 2104–2112.

[19] Y.S. Ho, G. McKay, Pseudo-second order model for sorption processes, Process Biochem. 34 (1999) 451–465.

[20] H. Zhang, Z. Jin, L. Han, C. Qin, Synthesis of nanoscale zero-valent iron supported on exfoliated graphite for removal of nitrate, Trans. Nonferrous Met. Soc. China 16 (2006) 345–349.

[21] C.M. Cirtiu, T. Raychoudhury, S. Ghoshal, Systematic comparison of the size, surface characteristics and colloidal stability of zero valent iron nanoparticles pre- and post-grafted with common polymers, Colloid. Surf. A: Physicochem. Eng. Aspects. A 390 (2011) 95–104.

[22] L. Legrand, A. El Figuigui, F. Mercier, A. Chausse, Reduction of aqueous chromate by Fe(II)/Fe(III) carbonate green rust: Kinetic and mechanistic studies, Environ. Sci. Technol. 38(17) (2004) 4587–4595.

[23] S.A. Kim, S.K. Kannan, K.J. Lee, Y.J. Park, P.J. Shea, W.H. Lee, H.M. Kim, B.T. Oh, Removal of Pb(II) from aqueous solution by a zeolite–nanoscale zero-valent iron composite, Chem. Eng. J. 217 (2013) 54–60.

[24] X.Q. Li, W.X. Zhang, Sequestration of metal cations with zerovalent iron nanoparticles—A study with high resolution X-ray photoelectron spectroscopy (HR-XPS), J. Phys. Chem. C 111 (2007) 6939–6946.

[25] R.T. Wilkin, M.S. McNeil, Laboratory evaluation of zero-valent iron to treat water impacted by acid mine drainage, Chemosphere 53(7) (2003) 715–725.

[26] L. Selwyn, Overview of archaeological iron: The corrosion problem, key factors affecting treatment, and gaps in current knowledge, in: J.A. Hallam (Ed.), Metal: Proceedings of Interim Meeting of the ICOM-CC Metal WG, National Museum of Australia, Canberra, 2004, pp. 294–306.

[27] Y.L. Zhang, Y.M. Su, X.F. Zhou, C.M. Dai, A.A. Keller, A new insight on the core–shell structure of zerovalent iron nanoparticles and its application for Pb(II) sequestration, J. Hazard. Mater. 263 (2013) 685–693.

[28] X. Zhang, S. Lin, X.Q. Lu, Z.L. Chen, Removal of Pb(II) from water using synthesized kaolin supported nanoscale zero-valent iron, Chem. Eng. J. 163 (2010) 243–248.

[29] X.F. Yun, M. Megharaj, N. Ravendra, Reduction and adsorption of Pb^{2+} in aqueous solution by nano-zero-valent iron—A SEM, TEM and XPS study, Mater. Res. Bull. 45 (2011) 1361–1367.

[30] S.M. Ponder, J.G. Darab, T.E. Mallouk, Remediation of Cr(VI) and Pb(II) aqueous solutions using supported, nanoscale zero-valent iron, Environ. Sci. Technol. 34 (2000) 2564–2569.

[31] X. Zhang, S. Lin, Z. Chen, Kaolinite-supported nanoscale zero-valent iron for removal of Pb^{2+} from aqueous solution: Reactivity, characterization and mechanism, Water Res. 45 (2011) 3481–3488.